Optically produced true-time delays for phased antenna arrays

Betty Lise Anderson, Stuart A. Collins, Jr., Elizabeth A. Beecher, Charles A. Klein, and Stephen B. Brown

A device is described for generating true-time delays optically for microwave signals used in beam steering and beam shaping in phased-array antennas. The device can be adapted to provide delays from picoseconds to nanoseconds. A single, compact unit should provide parallel delays for more than 64 independent antenna elements with a greater than 6-bit resolution. The time delays are produced by multiple reflections in a mirror configuration with continuous refocusing. A single spatial light modulator selects independent optical path lengths for each of the parallel antenna elements. Amplitude control for beam shaping can be integrated into the device. The unit can be made rugged for harsh environments by use of solid-block construction. The operation of the true-time delay device is described, along with the overall system configuration. Preliminary experimental data are given.

Key words: True-time delay, phased-array antennas.

1. Introduction

Phased-array antennas have the potential for a wide variety of applications from surveillance, tracking, astronomy, and geodesy to wireless and satellite communication. Phased-array antennas consisting of a number of independent, small-element antennas can be electronically scanned by reprogramming the way in which signals of the individual elements are combined.

The performance of phased arrays so far, however, has been limited because phase-shifting electronics are intrinsically narrow band. By replacement of phase shifts with true-time delays (TTD's), signals from different elements can be correlated independently of frequency. Electronically implementing the TTD is generally impractical because of the need for many long lengths of strip line, waveguides, or coaxial cable, which are expensive, bulky, and temperature sensitive. Because long paths are comparatively easy to obtain optically, photonic systems promise a means of obtaining the beam agility of array systems combined with wide bandwidth.

Approaches to optical TTD tend to fall into two categories: those using fibers[1–11] and those using long free-space paths.[11–16] Some fiber approaches use multiple optical switches or broadcast the light over all possible paths at once. Wavelength-division-multiplexing schemes have recently been developed by use of fiber Bragg gratings.[4,9] Free-space systems have also used multiple optical switches for switching the beams between sequential optical paths. These optical switches are usually liquid-crystal based.

We describe here a TTD device that falls into the free-space category but uses a multiple-pass optical cell with refocusing mirrors that has the advantage of avoiding beam-spreading problems. This approach differs from previous free-space approaches in that it uses only one optical switch or spatial light modulator (SLM) and one beam splitter, rather than one or more SLM's for each bit. The device controls a separate light beam for each antenna element and modifies the length of the path that each beam travels through the cavity. Many beams circulate through the cell simultaneously, and the length of the path that each beam travels is controlled independently. The amplitude of each beam is also independently adjustable for full phased-array beam shaping, and the device is fully reciprocal in that it can be used for either transmitting or receiving.

The authors are with the Department of Electrical Engineering, The Ohio State University, 205 Drecse Laboratory, 2015 Neil Avenue, Columbus, Ohio 43210.

Received 4 March 1997; revised manuscript received 27 June 1997.

0003-6935/97/328493-11$10.00/0

The optical TTD approach presented here has its roots in a three-mirror optical cell that was designed originally by J. White[17] for spectroscopic measurements requiring very long optical paths through a gaseous sample. The original White cell has been in common use in the spectroscopy community since its inception. White later made modifications for special applications.[18] The original White cell has also been used for time delays, either as a tapped delay line[19] or for pulse-train generation.[20] Other uses indirectly related to time delays include acoustic pulsing[21] and cineholography.[22] The White cell has even been adapted for optical computing.[23]

We start in Section 2 by describing the details of operation of the TTD device. In Section 3 we show how the device fits into an overall antenna system, and in Section 4 we present some preliminary experimental data from a working prototype. In Section 5 we discuss the expected performance capabilities, and in Section 6 we devote time to conclusions and a summary.

2. Theory of Operation

A. Introduction

The TTD device operates by allowing each of many independent beams to make a controlled number of passes back and forth through an optical cavity. The device is based on the White cell,[17] a simple optical cavity consisting of three spherical mirrors that recirculates a beam many times through the cell and refocuses the beam on each pass. The TTD device we describe here operates similarly but has extensions to achieve our purpose. First, it recirculates many beams simultaneously. Also, the time each beam spends bouncing back and forth in the cell is controlled independently by use of a single SLM. Then we use two cells of different optical path lengths but one mirror in common, that mirror being the surface of the SLM. This configuration increases the range of possible transit times.

In Subsection 2.B we begin by reviewing the operation of the original White cell. In Subsection 2.C we discuss the first modifications for the generation of variable TTD's including the incorporation of the SLM. Then in Subsection 2.D we describe the compound-cell approach to developing a practical TTD device, and in Subsection 2.E we improve the compound-cell device even further by making the mirrors different. In Subsection 2.F we show that this final design results in many more different delays times for the same number of beam transits through the cell. In Subsection 2.G we show how integrated amplitude control can be implemented, and finally in Subsection 2.H we discuss some construction options that can make the device mechanically rugged.

B. Basic White Cell

A diagram of the original White cell is shown in Fig. 1. It consists of three identical spherical mirrors, all of the same radius of curvature, as shown in Fig. 1(a).

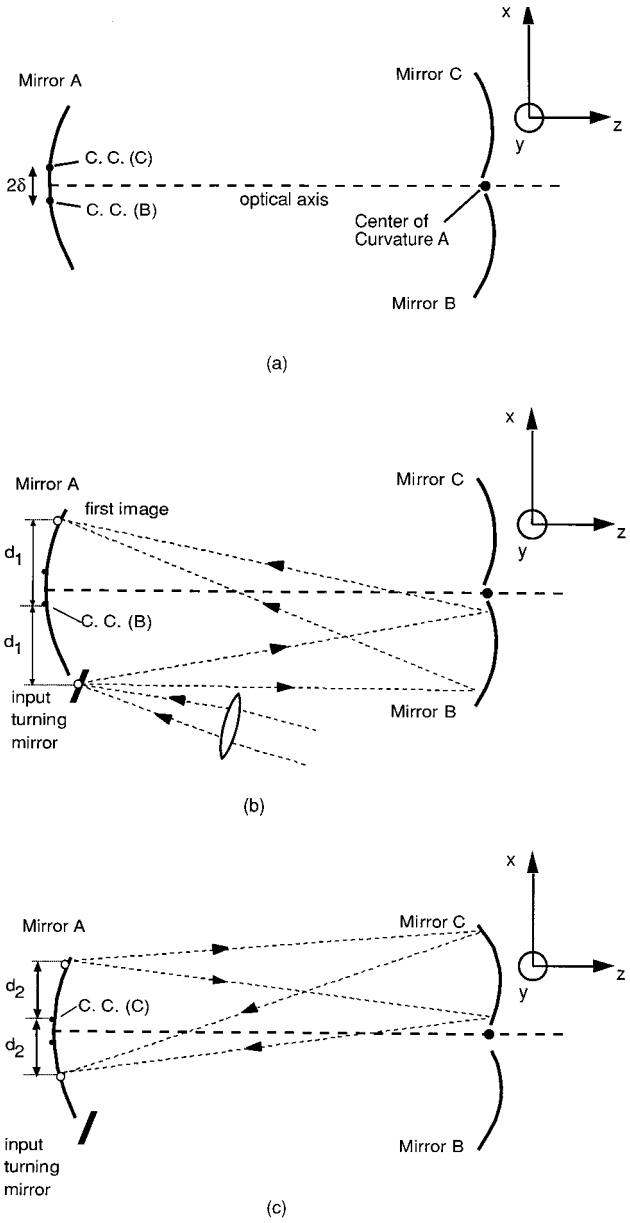

Fig. 1. (a) Basic White cell. (b) Operation of the White cell: The beam is introduced into the cell by means of an input turning mirror, expands to fill mirror B, and is imaged to a point again on mirror A. (c) The beam expands again, this time filling mirror C, and is focused to a new point on mirror A. C. C., center of curvature.

Mirror A is separated from mirrors B and C by a distance equal to their radii of curvature. The center of curvature of mirror A lies on the optical axis and falls between mirrors B and C. The alignment of mirrors B and C is such that their centers of curvature land on mirror A, each a distance δ from the optical axis. Light from mirror B is imaged by mirror A onto mirror C and vice versa.

During operation light enters the White cell from a spot imaged onto a small, flat mirror called the input turning mirror, as shown in Fig. 1(b). The input light beam is prepared so that it expands to fill mirror B. Mirror B refocuses the beam to a point on mirror

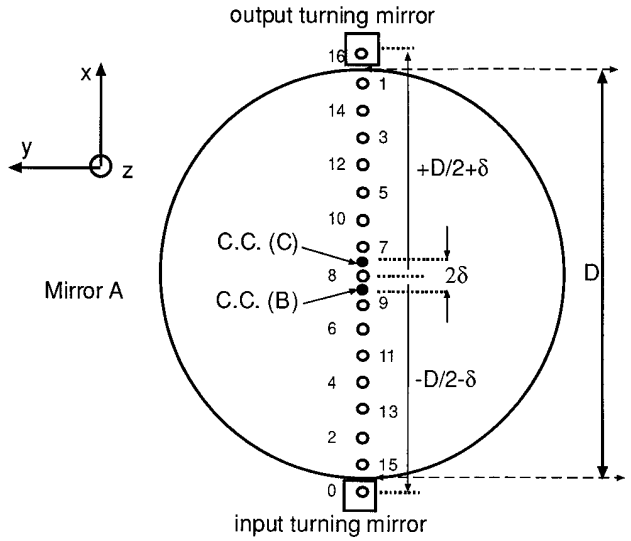

(a)

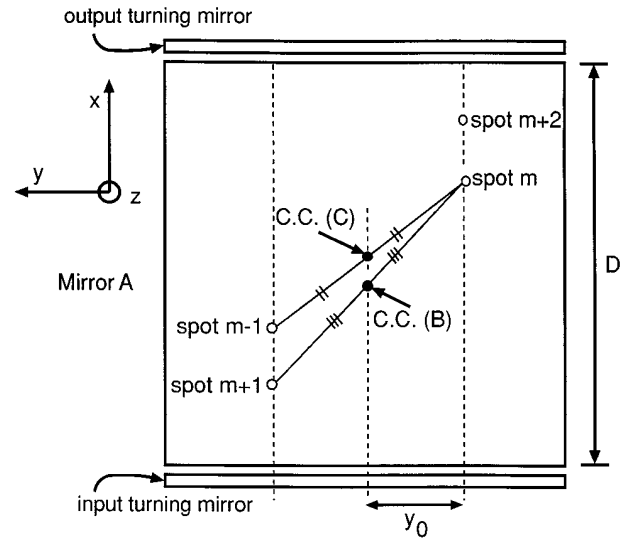

(b)

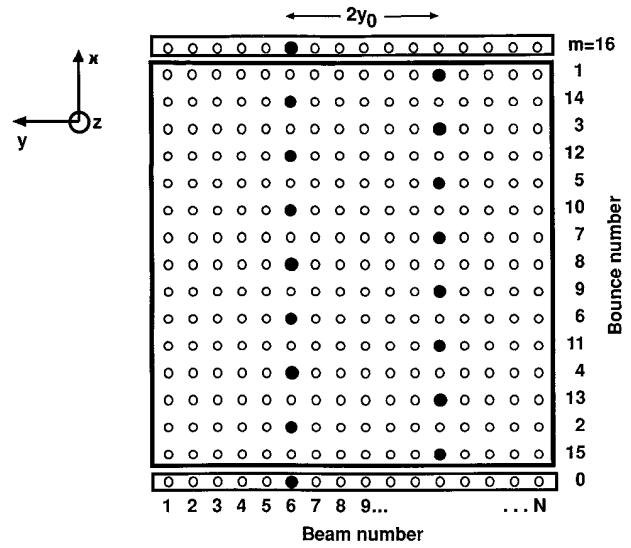

(c)

A. If the beam enters the cell at a distance d_1 from mirror B's center of curvature, it will be focused to a point the same distance d_1 on the opposite side of the center of curvature. From there, the beam is reflected by mirror A, expands again, and just fills mirror C, as shown in Fig. 1(c). Since the point being imaged by mirror C is located a distance d_2 from the center of curvature of mirror C, that mirror refocuses the light beam to a new spot a distance d_2 away from mirror C's center of curvature on the opposite side.

This process continues as shown in Fig. 2(a), which is drawn from the perspective of looking at mirror A from the right-hand side of Fig. 1. The centers of curvature of mirrors B and C are shown, and the spots, alternating from top to bottom of mirror A, are numbered in the sequence in which they appear. The optical axis is at the center of the figure, coinciding with spot 8. The spots eventually miss mirror A. The number of total bounces is determined directly by the spacing 2δ between the centers of curvature of mirrors B and C and by the overall size D of mirror A.

It is possible to extend the original White cell to include more than one beam of light. Suppose a particular input beam is not introduced on a line that contains the centers of curvature of mirrors B and C, as it was shown in Fig. 2(a). When an input beam is introduced off that line, say, by an amount y_0 as shown in Fig. 2(b), the spots alternate from top to bottom *and* left to right. Mirror A is now shown as a square rather than round section of a spherical mirror. Also, the turning mirrors have been extended.

We can predict the location of each successive spot. Suppose the spot on the input turning mirror is located a distance $-D/2 - \delta$ from the optical axis in the x direction and at a distance $-y_0$ in the y direction. Successive bounces will appear at locations given by

$$(x_m, y_m) = \left\{\left[-\frac{D}{2} + (2m-1)\delta\right], -y_0\right\}, \qquad m \text{ even},$$
$$(x_m, y_m) = \left\{\left[+\frac{D}{2} - (2m-1)\delta\right], y_0\right\}, \qquad m \text{ odd}, \tag{1}$$

It is possible to use the entire area of mirror A. Figure 2(c) shows mirror A with a series of input spots introduced at the input turning mirror at the bottom of the figure. The darkened spots are those corresponding to beam 6 on the turning mirror. The individual beams maintain their independence, each tracing out a unique sequence of spots. No two beams ever strike the same point on this mirror during the progression.

Fig. 2. (a) Sequence of spots for an input beam in line with the centers of curvature of mirrors B and C. The optical axis intersects the mirror at its center, coincident with spot 8. (b) Construction used to predict the location of the next spot. The mirror has been made a square section of a spherical mirror. (c) An array of input beams, with beam 6's sequence highlighted.

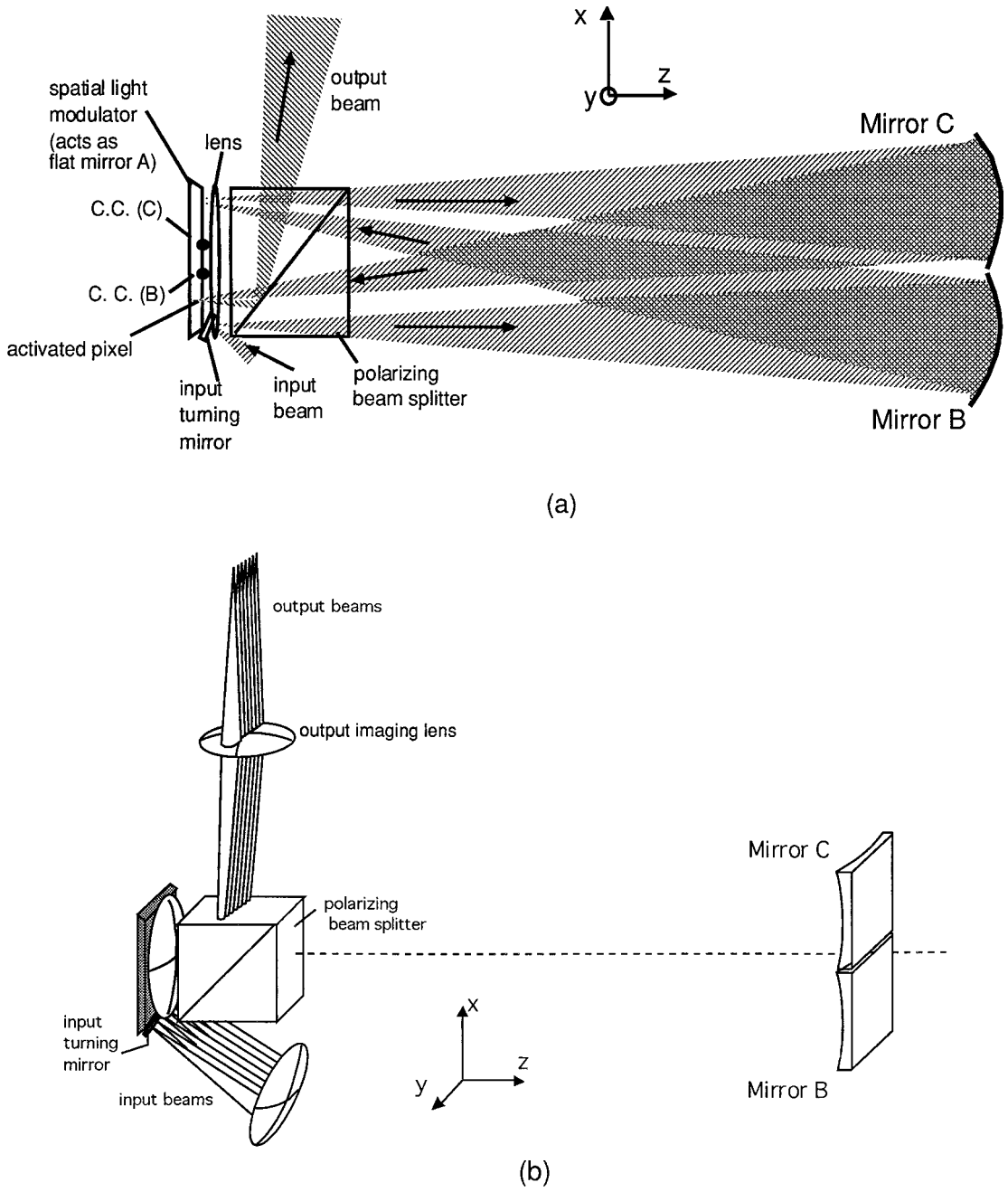

Fig. 3. (a) Type I cell: One beam is shown making two full transits of the cell, or twice the minimum path. (b) Three-dimensional view of a type I cell showing multiple beams. One beam will be used for each antenna element in the radar array.

C. Modifications to the White Cell

We now make our first set of modifications to the White cell to adapt it to variable TTD applications. The modifications are shown in Fig. 3(a). The first modification is to change mirror A from a curved mirror to a flat one and to add a lens of focal length f, where f is equal to the radius of curvature of the original spherical mirror. In this case the lens–mirror combination is optically equivalent to the mirror it replaces. Next, we replace the flat mirror (mirror A) with a reflective SLM. The SLM, which can be either electronically or optically addressed, is configured to rotate the direction of polarization of the reflected beam by 90° at any particular pixel that is activated. Finally, we add a polarizing beam splitter, adjusting the distances to mirrors B and C to maintain imaging. We require the input light to be polarized in the plane of the paper of Fig. 3(a). The beam splitter reflects light polarized in the plane perpendicular to the paper but transmits light polarized parallel to the plane of the paper. In this way, light reflecting from an activated pixel is turned out of the cell. We refer to a cell with these modifications as type I.

We are interested in the time delays experienced by the light pulses propagating through the cell. We

see that the time delays are in units of the transit time $T_{A(B,C)}$ from mirror A (now the SLM) to either mirror B or mirror C and back, where

$$T_{A(B,C)} = \frac{2[R + (n-1)S]}{v} \text{ (seconds)}, \qquad (2)$$

where R is the distance between mirror A and either mirror B or C, n is the refractive index of the beam-splitter cube, S is the length of the cube, and v is the velocity of light in free space.

We can now start to make the connection with phased-array microwave antennas. Phased antenna arrays require many independently variable time delays, so we introduce multiple light beams into the TTD device, as shown in Fig. 3(b). We associate one light beam with each antenna element. The TTD device then simultaneously generates independent delays for each antenna element. Addressing the appropriate pixel of the SLM allows each of these light beams to be made to transit the cell a different number of times. The beams entering the cell are all polarized such that they pass through the beam splitter unaffected. When a particular pixel on the SLM is addressed to rotate the beam polarization, the beam is then reflected by the beam splitter rather than transmitted and is turned out of the cell. For example, the beam shown in Fig. 3(a) is turned out after two reflections off the SLM.

The type I approach has difficulties with respect to the output optics because the beam leaves the time-delay cell from a different point and at a different angle, depending on the particular delay chosen. Although we have designed the required output optics, they are cumbersome and actually are not needed because a better cell design exists, as described in Subsection 2.D.

D. Compound Cell

One can implement a better TTD photonic device by next adding a second pair of identical spherical mirrors (call them E and F), as shown in Fig. 4. We refer to this configuration as type II. Mirrors E and F have the same focal lengths, but these are different from those of mirrors B and C.

Now we have dual cells, joined at the beam splitter. A single lens next to the SLM cannot satisfy the focusing conditions for both the cell containing mirrors B and C and the cell of mirrors E and F. We solve this problem by using two different lenses of focal lengths f_1 and f_2, which are now moved to the output sides of the polarizing beam splitter. The focal lengths are chosen to compensate for the new lens and mirror locations.

In the type II device of Fig. 4 there are different transit times in the two cells because of their different path lengths. In this configuration instead of ejecting a given beam after a predetermined number of transits, each beam makes the same total number of transits through the device. Now, however, the SLM is used to control the number of those transits that are made to mirrors B and C and the number

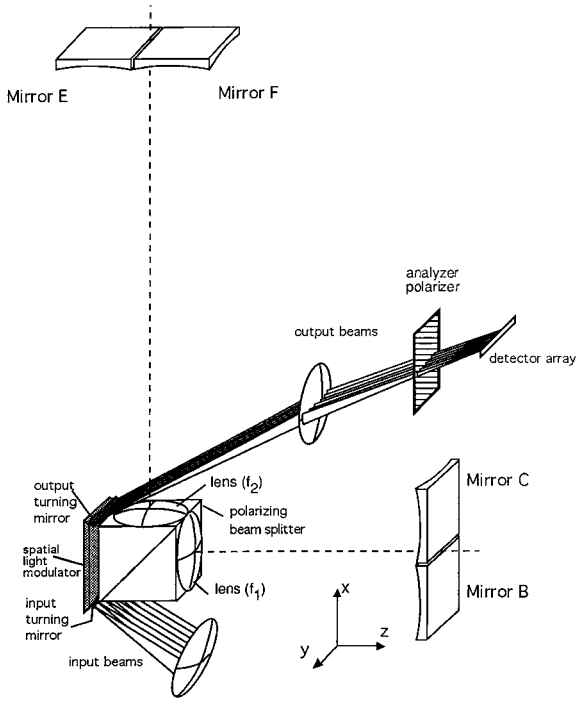

Fig. 4. Type II cell consisting of two type I cells that share the SLM as a common mirror and also share the beam splitter.

that are made to mirrors E and F. The minimum possible delay corresponds to a path having all the bounces through the shorter cell, and the maximum delay results from all passes traveling through the longer cell. The smallest delay increment Δ is the difference between the two-way path lengths through the shorter and longer cells:

$$\Delta = T_{A(B,C)} - T_{A(E,F)}, \qquad (3)$$

where the values of T are found by use of Eq. (2). The total differential delay is some integer multiple of that delay increment.

Making the radii of mirrors E and F nearly equal to the radii of mirrors B and C allows the differential time delay to be made small. Similarly, the delay difference can be quite large if the compound cell is more asymmetric. For this reason the device is suitable for quite small delays as well as large ones.

In the type II configuration every light beam makes the same number of trips through the device, even though the particular path varies with the delay chosen. Every beam makes a predetermined number of spots on the SLM and leaves the cell from a point on the output mirror as determined only by that beam's entrance point on the input turning mirror. Thus the optics required, for example, in the transmit mode to couple the outputs to the antenna elements (or the corresponding optical fiber in the case of remoting), are fixed and identical regardless of the total delay selected.

E. Final True-Time Delay Device

We make one further modification: We remove the restriction that the two focusing mirrors in each cell be identical. We can thus obtain many more delay increments for a given number of bounces. Figure 5 shows this final configuration—call it type III—for the case in which mirrors E and F have different focal lengths. Mirrors B and C could also be made different from each other but are shown the same in the figure without loss of generality. Again, lens f_2 is chosen to satisfy the new imaging conditions.

We point out that, although the lenses are different for the two arms, the imaging is still 1:1 for any of the paths, so that each light beams hits the SLM in the same sequence of spots regardless of which path that beam follows in the dual cell. Also, each beam again exits the cell at a fixed location, independent of the delay.

To determine the attainable time delays, we begin by examining the possible paths of the beams. From the input turning mirror the geometry is such that all beams must go to mirror B. From mirror B the beams return to the SLM, completing the first transit, at which point their individual polarizations are either rotated or not. If the polarization of a particular beam is not rotated on the first bounce it proceeds to mirror C. If the polarization *is* rotated the beam goes to mirror F. After the second transit each beam can go either to mirror B or E, again on the basis of whether the corresponding pixel on the SLM is activated.

We next label the mirrors as odd or even, depending on the number of the bounce from the SLM. Thus mirrors B and E are even since the beam can visit these mirrors only after an even-numbered bounce, and similarly mirrors C and F are odd. Light leaving an odd mirror can be directed only to an even mirror, and vice versa. A transition diagram is shown in Fig. 6. Let m be the number of times each independent beam travels from the SLM (or input turning mirror) to any one of mirrors B, C, E, or F and back to the SLM. For example, $m = 16$ in Fig. 2(c). In our device the symmetry is such that m will always be an even number; thus there will always be $m/2$ bounces off the odd mirrors and $m/2$ bounces off the even mirrors.

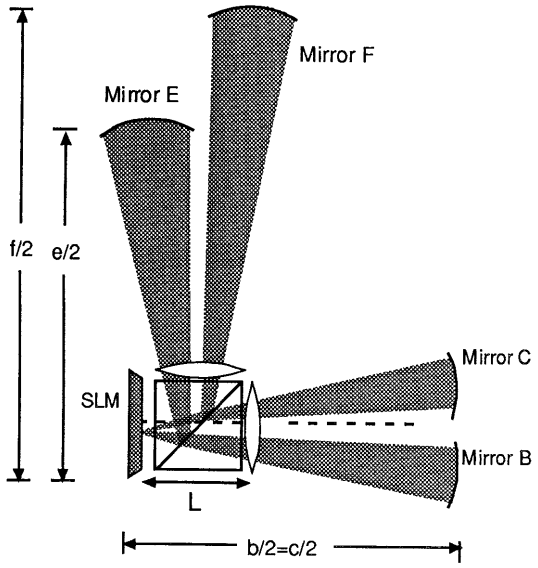

Fig. 5. Type III TTD device. The device shown here has a considerably greater range of time delays than does the type II device. The distances b, c, e, and f are optical path lengths.

F. Time Delays in the Final Device

We can now write the expressions for the transit time through the device. Let b, c, e, and f be twice the optical distance from the SLM to the corresponding mirror, as shown in Fig. 5. Also let i be the number of bounces off (even) mirror E and let j be the number of bounces off (odd) mirror F. Then there will be $(m/2 - i)$ bounces off the other even mirror, B, and $(m/2 - j)$ bounces off the other odd mirror, C. The values of i and j for any particular light beam are governed by the particular pixels activated on the SLM.

The total transit time is then given by

$$T = \frac{1}{v}\left\{ei + b\left[\left(\frac{m}{2}\right) - i\right] + fj + c\left[\left(\frac{m}{2}\right) - j\right]\right\}$$
$$= \frac{1}{v}\left\{(b + c)\frac{m}{2} + (e - b)i + (f - c)j\right\}. \quad (4)$$

Equation (4) shows that the total transit time has a constant portion,

$$T_0 = \frac{1}{v}(b + c)\frac{m}{2}, \quad (5)$$

and a variable portion,

$$T_v = \frac{1}{v}[(e - b)i + (f - c)j]. \quad (6)$$

Equation (6), the controllable delay time, depends on only the two path differences $(e - b)$ and $(f - c)$ and the selection of i and j.

The allowed range of time delays is determined by the counters i and j. For the odd mirrors either

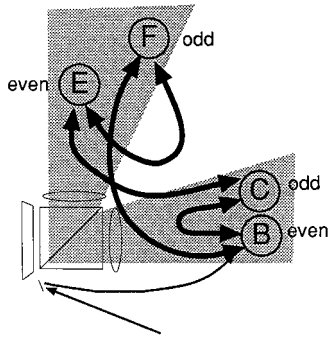

Fig. 6. Transition diagram showing the allowed progressions of the beams from mirror to mirror. The beam must always go to mirror B after the input turning mirror (bounce zero).

mirror C or F can be selected each time, so that counter j can range from 0 to $m/2$. For the even mirrors, the beam must first go to mirror B; mirror E cannot be selected until after the beam has struck the SLM at least once. Mirror E can thus be selected a maximum of $m/2 - 1$ times, so the counter i can range from 0 to $m/2 - 1$.

We now wish to optimize Eq. (4) to provide the longest complete sequence of delays for a given number of transits m. Let us assume that $e > b$ and $f > c$. Thus the minimum possible total delay will be obtained if all bounces are between mirrors B and C, that is, $i = j = 0$. All paths will have at least this minimum delay T_0 in common. The next possible shortest delay would be obtained if the beam were diverted to the even mirror having the longer focal length one time, that is, it goes to mirror E instead of mirror B on one of the even passes, or $i = 1$ and $j = 0$. Here we have assumed that $(f - c) > (e - b)$. Note that the beam still visits mirror C on every odd pass.

For a given desired delay increment Δ, we choose the focal lengths of mirrors E and B such that

$$\frac{1}{v}(e - b) = \Delta. \tag{7}$$

For delays of Δ, 2Δ, 3Δ, etc. to be produced, the beam is deflected to mirror E the corresponding number of times, which is accomplished by incrementing i. The maximum value that i can attain, however, is $m/2 - 1$, giving a delay of $(m/2 - 1)\Delta$. To continue the sequence, then, one would like to increment j, the number of visits to the longer-focal-length odd mirror, and reset i to zero. Recall our assumption that $f > c$. Thus one chooses the focal lengths of mirrors F and C such that

$$\frac{1}{v}(f - c) = \frac{m}{2}\Delta. \tag{8}$$

In effect we are counting in a base $(m/2)$ system, where i is the digit in the ones place and j is the digit in the $(m/2)$'s place, which is the next significant digit.

Note that there are no particular constraints on the actual choices of lengths b, c, e, and f, only on the differences $e - b$ and $f - c$. Therefore, to keep the overall device size as small as possible, it is advantageous to make b and c as small as possible, thereby keeping e and f small. As long as the difference $e - b$ is the appropriate length with respect to $f - c$, the lengths can be chosen at will.

The maximum possible delay results when the beam passes from mirror E to mirror F and back as often as possible, so that there are $j = m/2$ trips to mirror F and $i = m/2 - 1$ trips to mirror E. The maximum time delay is therefore

$$T_{\max} - T_0 = \left(\frac{m}{2} - 1\right)\Delta + \left(\frac{m}{2}\right)\left(\frac{m}{2}\Delta\right) = \frac{(m^2 + 2m - 4)}{4}\Delta. \tag{9}$$

We see that the maximum delay goes quadratically as the number of bounces. For 16 bounces, 72 different individual delays, from 0 to 71Δ, are possible. A straightforward algorithm exists to find the sequence required to produce any particular integer multiple of the delay Δ.

G. Amplitude Control

For complete control of a radar beam, one wants, in addition to TTD's, control of the amplitude of the signal sent by each antenna element for purposes of beam shaping and nulling. In the TTD devices described here the amplitude control can be integrated directly into the TTD device by instruction of the SLM to elliptically polarize each beam just before it leaves the cell, as shown in Fig. 4. This change to elliptical polarization is accomplished by the application of appropriately less than that input required for a change from horizontal to vertical linearly polarized light, so that the analyzing polarizer transmits the desired amplitude at the output. The appropriate control signal is applied to the pixels in the last row on the SLM, for example, row 15 in Fig. 2(c), so that the last bounce is used for amplitude control of each beam rather than for timing. If amplitude control is implemented, the total number of delays is reduced slightly since the last bounce on the SLM cannot be used for choosing a path.

H. Construction Options

For a slightly different configuration, the optical path lengths in the two cells can also be made different by variation of the refractive index of the material between the beam splitter and the mirror pairs. Moreover, the unit can be made rugged by use of a solid material instead of air, as shown in Fig. 7. There we see a possible solid-block construction. The spherical mirror surfaces can be ground onto the ends of the glass or other optical material, and those surfaces can then be coated for enhanced reflectivity. Some change in material will be necessary to produce the lenses at the outputs of the beam splitter. This solid construction is appealing because it is rugged and could be made comparatively temperature insensitive.

3. System Configuration

Figure 8 shows how the TTD device would fit into a phased-array antenna system. We see two configurations, one for transmitting and one for receiving. Our optical TTD device is shown in the centers of Figs. 8(a) and 8(b). There is one beam through the

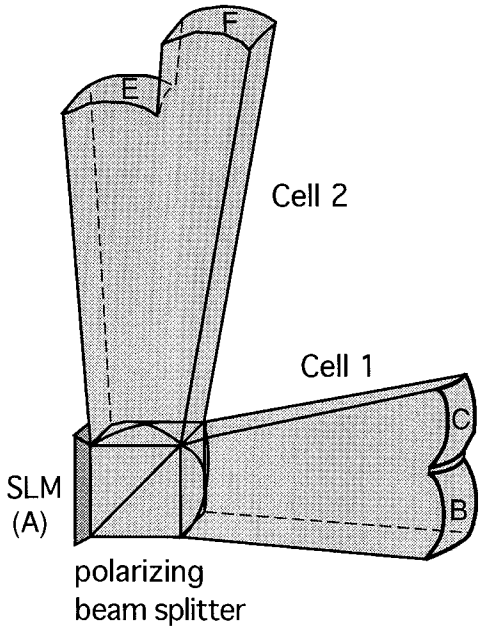

Fig. 7. Solid-block construction of the TTD device, shown for the type III device.

device for each antenna element; each beam is independently delayed and amplitude controlled.

In the transmit mode, shown in Fig. 8(a), a separate polarized and rf-modulated light beam is introduced into the cell for each of N antenna elements. The N beams can be generated by N lasers or by use of a $1 \times N$ splitter as shown in the figure, and a single rf-modulated laser beam. The light source(s) can be of any single wavelength and need not necessarily be lasers since the TTD device will work for incoherent as well as coherent light.

The N identical rf-modulated light beams are introduced into the TTD device. The beams are given the N individual time delays associated with the desired steering angle. Each independently time-delayed beam is detected by a photodetector that drives a transmit module (amplifier and antenna array element). The amplitude of each light beam is adjusted individually for antenna beam shaping.

Figure 8(b) shows the receive case, in which N array-element signals modulate N independent light beams. The beams are input into the TTD device and are delayed individually to form the desired receive pattern. The amplitude control can be used for null steering during this receive preprocessing operation.

4. Experiment

We have built a proof-of-concept type I device (refer to Fig. 3) and demonstrated controllable TTD's of a laser beam, measured in the time domain. The experimental apparatus is shown in Fig. 9(a). The SLM is a Hughes liquid-crystal light valve (LCLV) that is addressed optically by use of a collimated incandescent light source and a scanning slit. The spherical mirrors have a multilayer dielectric-coated front surface and a radius of curvature of 500 mm. The lens to the right of the beam splitter has a focal length of 400 mm. The lens is located 400 mm from the spherical mirrors and 123 mm from the reflecting surface of the LCLV. This takes into account the optical thickness of the beam splitter and the light valve.

The turning mirror(s) must be in the same plane as the reflecting surface of the LCLV, which is not physically possible with this light valve because that surface is buried behind a half-inch glass substrate. We therefore use an additional mirror, called an auxiliary mirror, located above the LCLV. Spots on the LCLV are imaged onto the auxiliary mirror by means of mirror C, and spots on the auxiliary mirror are

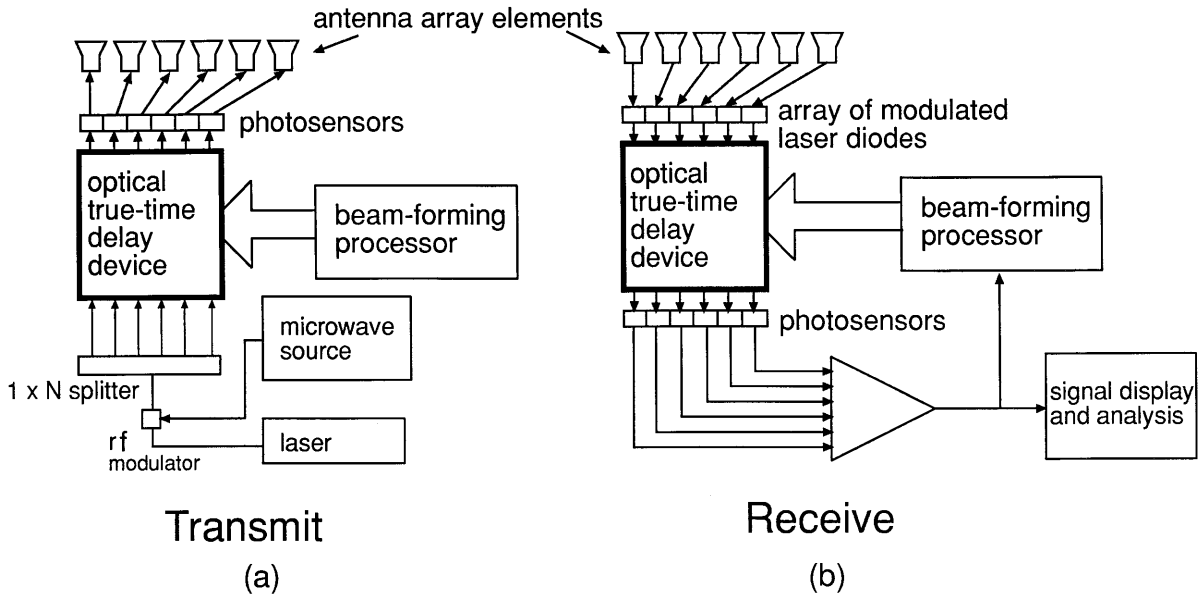

Fig. 8. (a) Transmit microwave TTD system configuration. (b) Receive microwave TTD system configuration.

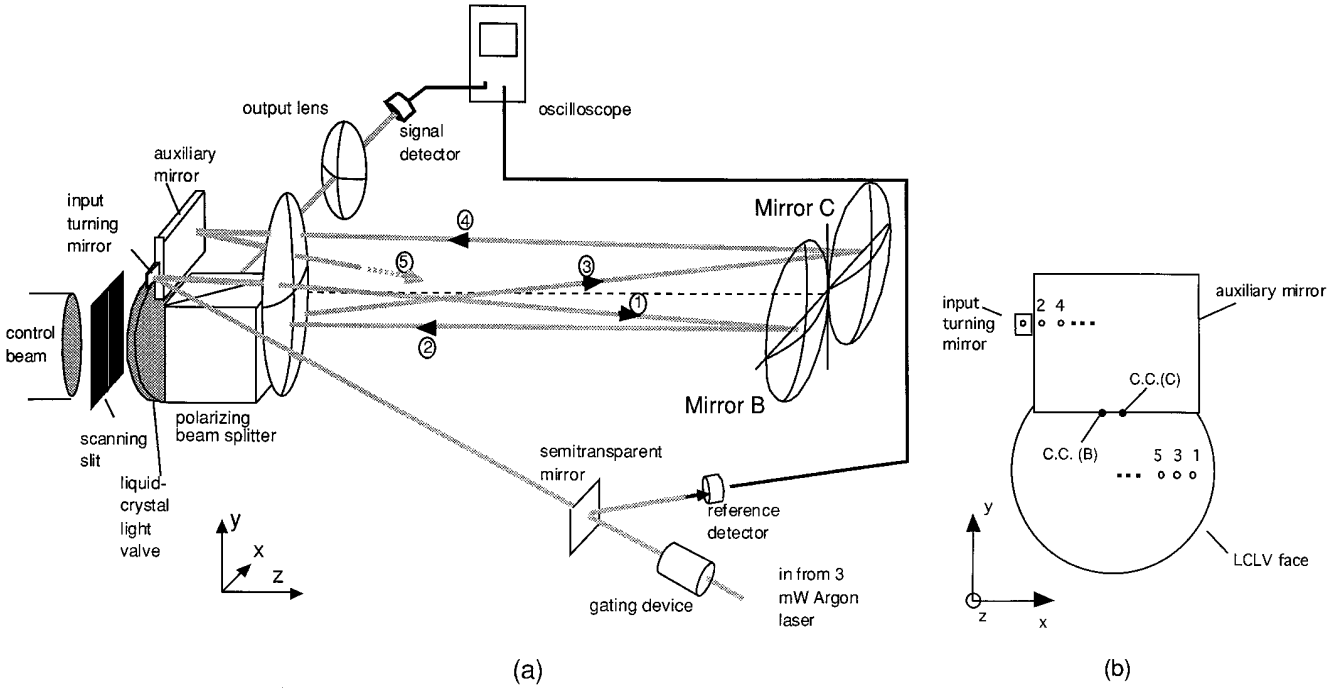

Fig. 9. (a) Experimental apparatus. (b) Front view of the light valve and auxiliary mirror.

imaged back onto the light valve by means of mirror B, as shown in Fig. 9(b). The polarizing beam splitter is located in front of the LCLV, and light is ejected from the system only after it bounces off the LCLV. For this reason our demonstration cell was limited to delays that were multiples of two round trips through the cell.

The light beam being delayed was a green beam from a 3-mW argon laser, $\lambda = 514$ nm. It was pulsed by use of an external Pockel's effect optical gating device that produced ~250-ns pulses with a less than 1-ns rise time. A portion of the optical power was diverted for triggering by use of a beam splitter. The trigger detector was a Thor Laboratories Model DET1-S1 p-i-n detector, followed by a Hewlett-Packard Model 462A amplifier. The signal detector was a Newport Model 877 avalanche photodiode, used with a Hewlett-Packard Model 461A amplifier.

The pulsed laser beam enters the cell by means of the input turning mirror and bounces back and forth in the cavity until it strikes an activated pixel on the LCLV. Then the beam is reflected by the polarizing beam splitter and strikes the photodetector. One selects the number of bounces the beam makes in the cell by moving a slit across the back of the LCLV to illuminate the appropriate pixel. The row of spots from the SLM is imaged onto the detector plane. For this simple demonstration, a single detector is moved to each spot to measure the corresponding delay.

The digital oscilloscope, Hewlett-Packard Model 54501A, compares the delayed beam to the trigger beam. Figure 10 shows an undelayed beam superimposed with three separately delayed beams. The lower trace is the trigger signal. The signals are inverted, and only the leading edges of the pulses are shown. Each trace is an average of 60 pulses. The large number of pulses was necessary only because of the speed limitations of the sampling oscilloscope. The sweep rate is 5 ns/division, and the delays are measured to be 0, 7.2, 14.0, and 21.3 ns, respectively. This gives an average delay difference of 7.1 ns. The measurement error is approximately ± 1.2 ns, meaning our measured delay matches the predicted delay, based on physical measurements of the path, of 6.8 ns.

5. Performance

We next address the factors determining the range of delays, delay resolution, number of beams supported, and switching speed. First, the cumulative power losses resulting from imperfect reflection limit the total number of independent delays per beam. The greatest source of loss is expected to be at the polarizing beam splitter, which has a transmission factor T_p for p-polarized light and reflection factor R_s for s-polarized light. The losses, typically of the order of 0.03 at the beam-splitting surface, are experienced on each pass through the beam splitter, that is, twice per cell transit. Properly coated mirrors and lenses will have losses of the order of 0.005 or better. For a single transit from the SLM to an opposing mirror and back, a given beam leaves the spherical mirror (transmission of 0.995), crosses the input and output faces of the beam splitter and lens twice each (transmission of 0.995^8), crosses the input face of the SLM twice (0.995^2), reflects off the back surface of the SLM once (0.995), and suffers some attenuation at the beam-splitting surface itself (0.97^2). The resulting worst-case total loss in one transit is $1 - (0.995)^{12}$ $(0.97)^2$, or approximately 11%. For 16 transits (72 delay increments), that results in a total transmis-

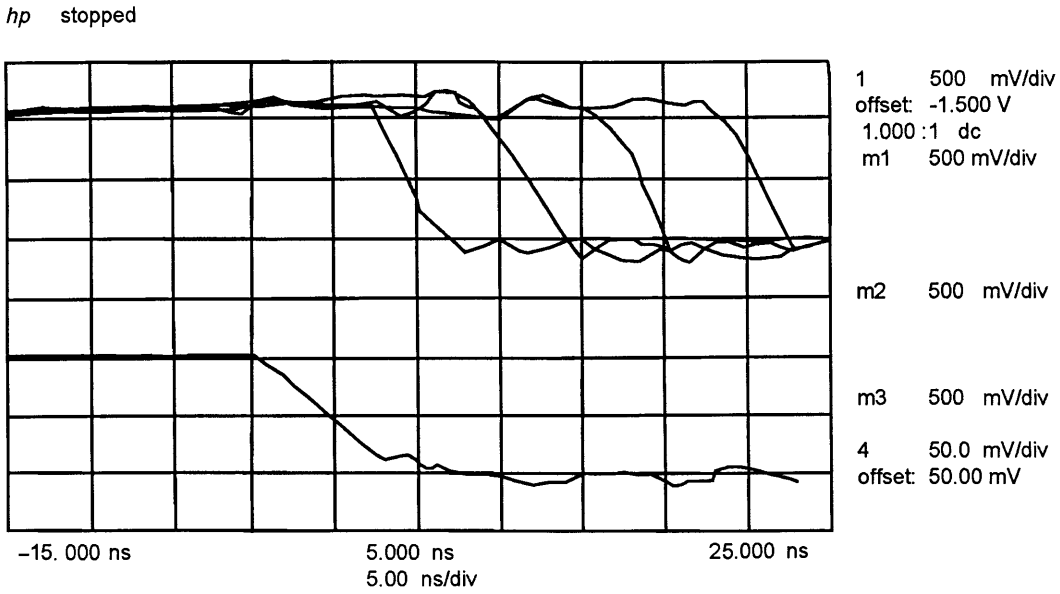

Fig. 10. Experimental data: four successive delays of 0, 7.2, 14.0, and 21.3 ns. There are five traces: channels 1 and 4 and memories m1, m2, and m3. Div, division.

sion of 0.15 (−8.2 dB), which is reasonable. There may be some additional loss that is due to scattering by the liquid-crystal molecules in the SLM, as well. This has not been well characterized since loss is not an issue in typical SLM applications.

Whereas the number of bounces is limited by the transmission losses, the number of independent beams is determined by the SLM's size and resolution. Suppose the pixel size is chosen to be 150 μm, a conservative value for which there is no interaction between light-valve pixels. Then an area on the SLM of 9.6 mm × 2.4 mm on a side is sufficient to process 64 beams in parallel. Commercially available SLM's of 25.4 mm on a side can therefore be used to process 25.4/0.15 = 169 independent light beams to drive 169 antenna elements. Alternatively, if a multiple-beam antenna application is required, the 169 independent light beams could be used in a multibeam fashion. If there were only 42 antenna elements, then four entirely different beams, each of which has full direction and shape control, could be produced.

One concern with the White cell historically has been astigmatism,[24–26] which is a consideration in spectroscopy when the number of cell transits can be in the hundreds. The TTD device presented here requires a comparatively small number of refocusings, and indeed we have not observed any noticeable distortion in our experiments. The small number of transits (~16) and relatively short cell lengths also make the TTD device far less susceptible to alignment errors and vibrations compared with spectroscopic White cells, which may use 10-m cell arms and hundreds of bounces.[18]

The lengths of the delay increments are determined by the optical distance to the mirror pairs from the SLM. To get long differential delays, of the order of nanoseconds, one would choose one cell of the device to have a long path and the other cell to have as short a path as possible. A long path could be folded around the outside of the smaller path in the interest of compactness. For smaller delays the two cells would be designed to be close in dimensions or to use materials of different refractive indices. Delay increments less than 10 ps should be possible.

The time required to switch between beam-steering directions is determined by the switching time of the SLM. There are various SLM technologies available[27] with different switching speeds. Response times of 50 μs have been measured for ferroelectric liquid crystals (FLC's),[28,29] and response times as fast as 13 μs are predicted for FLC's.[30] The FLC's have the low loss associated with liquid crystals and can be made in arrays as large as 256 × 256 pixels. Contrast ratios of 80:1 have been measured.[31] It should be noted that FLC SLM's are binary and cannot produce the required partial polarization change for amplitude control.[30]

6. Summary

We have described a photonic TTD device that easily could, using commercially available components, produce 64 different delay times (6-bit resolution) for 169 separate signals in parallel, with integrated amplitude control. The TTD device uses two optical cells that have one reflective surface in common, the SLM. One light beam for each antenna element circulates in the cells and is constantly refocused as it progresses. The common reflective device is a SLM that directs a given beam into one cell or the other by rotating the plane of polarization. A polarizing beam splitter transmits the beam into one cell or reflects it into the other. Choosing the number of times a given beam goes into each cell allows various lengths of time delays to be obtained.

Each of the two optical cells has two focusing mirrors in addition to their common SLM and polarizing beam splitter. We have shown that, by making the mirrors' focal lengths the same in one cell but different in the other, it is possible to produce approximately $m^2/4$ different time delays for m passes through the device.

Amplitude control can be integrated into the TTD device by use of the last bounce on the SLM for a partial polarization change rather than delay path switching. An analyzing polarizer at the detectors then passes the desired beam power.

We have demonstrated experimentally, as a proof of concept, a TTD unit that constitutes one half of the proposed device. We have shown three delays of $\sim$7 ns each; the delay increment is a function of the choice of mirrors. In practice, using the compound-cell TTD device could permit delays from a few picoseconds to many nanoseconds.

Among the advantages of this approach is the physical size of the TTD device, which is determined by the number of beams, the delay increment, and the SLM resolution. The constant refocusing in the cells means that diffraction over long optical paths does not imply an increase in the physical size of the unit. Other advantages include flexibility in light-source requirements, since there are no restrictions on source wavelength or coherence. The design is fully reciprocal in that it can be used equally well in the receive or transmit mode. Finally, this approach has the added benefit of integrated amplitude control for beam shaping and null steering. The design presented here can provide photonic TTD for the high-performance wideband phased-array antennas of the future.

References

1. J. J. Lee, R. Y. Loo, S. Livingston, V. I. Jones, J. B. Lewis, H.-W. Yen, G. L. Tangonan, and M. Wechsberg, "Photonic wideband array antennas," IEEE Trans. Antennas Prop. **45,** 966–982 (1995).
2. A. Goutzoulis, K. Davies, J. Zomp, P. Hyrcak, and A. Johnson, "Development and field demonstration of a hardware-compressive fiber-optic true-time-delay steering system for phased-array antennas," Appl. Opt. **33,** 8173–8185 (1994).
3. P. M. Freitag and S. M. Forrest, "A coherent optically controlled phased array antenna system," IEEE Microwave Guided Wave Lett. **3,** 293–295 (1993).
4. G. A. Ball, W. H. Glenn, and W. W. Morey, "Programmable fiber optic delay line," IEEE Photon. Technol. Lett. **6,** 741–743 (1994).
5. B. Kanack, M. Boysel, C. Goldsmith, C. Menni, G. Magel, and C. Takle, "Optical time delay network for phased arrays," in *Transition of Optical Processors into Systems*, D. P. Casasent, ed., Proc. SPIE **1958,** 114–132 (1993).
6. D. D. Curtis and L. M. Sharpe, "True time delay using fiber optic delay lines," in *Proceedings of the IEEE International Symposium Antennas and Propagation* (Institute of Electrical and Electronics Engineers, New York, 1990), pp. 766–769.
7. R. D. Esman, M. Y. Frankel, J. L. Dexter, L. Goldberg, M. G. Parent, and D. Stilwell, "Two optical-control techniques for phased array: interferometric and dispersive-fiber true time delay," *Transition of Optical Processors into Systems*, D. P. Casasent, ed., Proc. SPIE **1958,** 133–143 (1993).
8. D. J. Page, "An introduction to the optical commutator," IEEE Trans. Antennas Prop. **44,** 652–658 (1996).
9. D. A. Cohen, Y. Chang, A. G. J. Levi, H. R. Fetterman, and I. L. Newberg, "Optically controlled serially fed phased array sensor," IEEE Photon. Technol. Lett. **8,** 1683–1685 (1996).
10. N. A. Riza, "Polarization-based fiber optic delay lines," *Optical Technology for Microwave Applications VII*, A. P. Goutzoulis, ed., Proc. SPIE **2560,** 120–129 (1995).
11. N. A. Riza and N. Madamopoulos, "Phased-array antenna, maximum compression, reversible photonic beam former with ternary designs and multiple wavelengths," Appl. Opt. **36,** 983–996 (1997).
12. H. R. Fetterman, Y. Chang, D. C. Scott, S. R. Forrest, F. M. Espiau, M. Wu, D. V. Plant, J. R. Kelly, A. Mather, W. H. Steier, and G. J. Simonis, "Optically controlled phased array radar receiver using SLM switched real time delays," IEEE Microwave Guided Wave Lett. **5,** 414–416 (1995).
13. D. Dolfi, P. Joffre, J. Antoine, J. P. Huignard, J. Roger, and P. Granger, "Two-dimensional optical beam-forming networks," *Optoelectronic Signal Processing for Phased-Array Antennas IV*, B. Hendrikson, ed., Proc. SPIE **2155,** 205–217 (1994).
14. X. S. Yao and L. Maleki, "A novel 2-D programmable photonic time-delay device for millimeter-wave signal processing applications," IEEE Photon. Technol. Lett. **6,** 1463–1465 (1994).
15. N. A. Riza, "Transmit–receive time-delay beam-forming optical architecture for phased-array antennas," Appl. Opt. **30,** 4594–4595 (1991).
16. D. Dolfi, J. P. Huignard, and M. Baril, "Optically controlled true time delays for phased array antenna," *Optical Technology for Microwave Applications IV*, S.-K. Yao, ed., Proc. SPIE **1102,** 152 (1989).
17. J. White, "Long optical paths of large aperture," J. Opt. Soc. Am. **32,** 285–288 (1942).
18. J. U. White, "Very long optical paths in air," J. Opt. Soc. Am. **66,** 411–416 (1976).
19. E. O. Schulz-DuBois, "Generation of square lattice of focal points by a modified White cell," Appl. Opt. **12,** 1391–1393 (1973).
20. E. J. Beiting, "Compact optical pulse train generator," Appl. Opt. **31,** 2642–2644 (1992).
21. J. J. B. Deaton and J. W. Wagner, "Variable-cavity-length mode-locked Nd:YAG laser for noncontact and spectral control of narrow-band ultrasound," Appl. Opt. **33,** 1051–1058 (1994).
22. M. J. Ehrlich, J. S. Steckenrider, and J. W. Wagner, "System for high-speed time-resolved holography of transient events," Appl. Opt. **31,** 5947–5951 (1992).
23. S. A. Collins, Jr., J. Ambuel, and E. K. Damon, "Optics for numerical calculation," in *Proceedings of International Commission on Optics 11*, Madrid, Spain (International Commission on Optics, 1978).
24. T. R. Reesor, "The astigmatism of a multiple path absorption cell," J. Opt. Soc. Am. **41,** 1059–1060 (1951).
25. W. H. Kohn, "Astigmatism and White cells: theoretical considerations on the construction of an anastigmatic White cell," Appl. Opt. **31,** 6757–6764 (1992).
26. G. J. Rayl, "Multiple traversal absorption cell of minimum volume design," Appl. Opt. **15,** 921–928 (1976).
27. U. Effron, *Spatial Light Modulator Technology* (Marcel Dekker, New York, 1995).
28. N. Collings, J. Gourlay, D. G. Vaasl, H. J. White, C. Stace, and G. M. Proudley, "Measurements on ferroelectric liquid-crystal spatial light modulators: contrast ratio and speed," Appl. Opt. **34,** 5928–5931 (1995).
29. M. G. Roe and K. L. Schehrer, "High-speed and high-contrast operation of ferroelectric liquid crystal optically addressed spatial light modulators," Opt. Eng. **32,** 1662–1667 (1993).
30. A. Handschy, K. M. Johnson, G. Moddel, and L. A. Pagano-Stauffer, "Electro-optic applications of ferroelectric liquid crystal to optical computing," Ferroelectrics **85,** 279–289 (1988).
31. Displaytech, Inc., product literature (Boulder, Colo., 1996).